Mathematics

https://www.aimspress.com/journal/Math

AIMS Mathematics, 11(8): 26739–26764.
DOI: 10.3934/math.20261073
Received: 11 June 2026
Revised: 19 July 2026
Accepted: 23 July 2026
Published: 25 August 2026

Research article

Painlevé analysis and nonlinear wave structures of a variable-coefficient extended KdV equation in $(3 + 1)$ dimensions

Majid Madadi[1,2,3], **Yakup Yildirim**[3,4], **Udoh Akpan**[5] **and Lanre Akinyemi**[6,*]

[1] Department of Mathematics, Saveetha School of Engineering, Saveetha Institute of Medical and Technical Sciences, Saveetha University, Chennai 602105, Tamil Nadu, India

[2] Research Center of Applied Mathematics, Khazar University, Baku, Azerbaijan

[3] Mathematics Research Center, Near East University, 99138 Nicosia, Cyprus

[4] Department of Computer Engineering, Biruni University, Istanbul–34010, Turkey

[5] Department of Mathematics, West Texas A&M University, Texas, USA

[6] Department of Mathematics, Prairie View A&M University, Texas, USA

* **Correspondence:** Email: Laakinyemi@pvamu.edu.

Abstract: A variable-coefficient Korteweg–de Vries (KdV)-type equation in (3 + 1) dimensions is investigated with emphasis on Painlevé integrability and exact nonlinear wave dynamics. Using the Painlevé analysis, the model is shown to possess the Painlevé property under appropriate smoothness and nondegeneracy assumptions on the spatially varying coefficients. A Hirota bilinear representation is subsequently derived, from which an N-soliton solution is constructed. The model admits a variety of exact nonlinear wave structures, including multi-solitons, resonant Y-type waves, fusion and fission waves, X-type solitons, hybrid interaction patterns, and rational lump-type solutions in the admissible parameter regime. The spatially varying coefficients significantly modify soliton trajectories, resonant interaction geometries, and the locations of localized structures, while the exact solutions retain their asymptotic profiles and exhibit shape-preserving interaction patterns. The coexistence of exponential and rational wave structures highlights the richness of the solution space. These results enlarge the class of spatially inhomogeneous nonlinear evolution equations (NLEEs) exhibiting Painlevé–Hirota coherent-wave structures and provide analytical insight into nonlinear wave propagation in spatially inhomogeneous media.

Keywords: extended KdV equation; Painlevé analysis; Hirota bilinear; soliton solution; lump wave
Mathematics Subject Classification: 35Q51, 37K10, 37K40

1. Introduction

Nonlinear evolution equations (NLEEs) play an important role in applied mathematics and mathematical physics because they model nonlinear phenomena arising in shallow-water waves [1], plasma dynamics [2], nonlinear optics [3], and fluid mechanics [4]. Exact analytical solutions provide insight into the qualitative behavior of these systems and serve as useful benchmarks for numerical simulations and experimental investigations. Several analytical techniques have been developed for studying NLEEs, including Darboux transformations [5], the inverse scattering transform [6], Hirota's bilinear method [7], Painlevé analysis [8], Riccati-equation methods [9], generalized solitary-wave ansatz [10], and modified direct algebraic methods [11]. Among these approaches, Painlevé analysis and Hirota's bilinear method are particularly useful for identifying integrable structures and constructing multi-soliton, resonant, and rational wave solutions.

Solitons are localized nonlinear waves generated by a balance between nonlinear and dispersive effects. A characteristic feature of soliton solutions is their ability to preserve their profiles during propagation and, in integrable systems, after mutual interaction. Such structures arise in nonlinear optics [12], fluid dynamics [13], plasma physics [14], and optical communication [15]. Integrable nonlinear equations may also admit resonant Y-type waves, fusion and fission processes [16], and rationally localized lump solutions [17]. Painlevé analysis, introduced by Weiss, Tabor, and Carnevale (WTC) [18], examines the movable singularity structure of a nonlinear differential equation and provides strong evidence of integrability. Nevertheless, passing the Painlevé test alone does not establish complete integrability in the strongest sense; additional structures, such as a Lax pair, infinitely many conservation laws, a Hamiltonian formulation, or an inverse-scattering representation, may also be required.

Although constant-coefficient equations provide useful idealized models, many physical media are spatially inhomogeneous. Variations in material properties, external forcing, topography, temperature, and density can produce spatially dependent coefficients [19–23]. Variable-coefficient models arise naturally in oceanography [24], plasma physics [25], and nonlinear optics [26]. In such models, the coefficient functions may alter propagation trajectories, interaction geometries, phase shifts, and localization properties. At the same time, spatially varying coefficients make the analysis of integrability and exact solvability considerably more challenging.

Motivated by these considerations, we investigate the following variable-coefficient extended KdV-type equation in (3 + 1) dimensions:

$$\kappa_1(y)u_{xt} + 6\kappa_2(y)(uu_x)_x + \kappa_2(y)u_{xxxx} + \alpha\kappa_2(y)u_{tt} + \kappa_3(y)u_{xx} + \kappa_4(y)u_{xy} + \kappa_5(y)u_{xz} = 0. \tag{1.1}$$

Here, $u = u(x, y, z, t)$ denotes the wave field, α is a constant associated with second-order temporal dispersion, and the functions $\kappa_i(y)$ represent spatial inhomogeneity. The coefficient $\kappa_1(y)$ modulates the mixed space–time evolution, whereas $\kappa_2(y)$ controls the nonlinear and fourth-order dispersive terms. The coefficient $\kappa_3(y)$ introduces additional longitudinal dispersion, while $\kappa_4(y)$ and $\kappa_5(y)$ describe transverse coupling in the y- and z-directions, respectively. Thus, Eq (1.1) may be regarded as a generalized nonlinear-wave model for spatially inhomogeneous media rather than as a model restricted to a single physical setting.

When the coefficient functions are constant, Eq (1.1) reduces to the extended KdV-type equation introduced in [27]. Its constant-coefficient form has been investigated through Painlevé analysis,

N-soliton constructions, variational and Hamiltonian formulations, bifurcation analysis, periodic-wave theory, and chaotic dynamics [28, 29]. Multi-soliton and higher-order lump solutions have also been obtained using Hirota–Wronskian and bilinear techniques [30]. Related variable-coefficient KdV-type equations were considered in [31–33]. However, their exact solvability generally depends on restrictive relationships among the coefficient functions. To the best of our knowledge, a unified treatment combining Painlevé analysis, a variable-coefficient Hirota bilinear formulation, a general N-soliton hierarchy, resonant interaction structures, and rational lump-type solutions has not previously been reported for the present (3 + 1)-dimensional model. This gap motivates a systematic investigation of whether Eq (1.1) retains the coherent-wave structures of its constant-coefficient counterpart under sufficiently general spatial modulation.

The principal contribution of the present work is a combined Painlevé–Hirota analysis of Eq (1.1) for sufficiently smooth spatial coefficient functions. First, the equation is shown to possess the local Painlevé property on intervals where $\kappa_2(y) \neq 0$. Second, a Hirota bilinear representation is derived, and a general N-soliton solution is constructed under the additional nondegeneracy condition $\kappa_4(y) \neq 0$. The resulting formulation generates one-, two-, three-, and four-soliton solutions, together with resonant Y-type waves, fusion and fission processes, X-type solitons, and hybrid interaction patterns under suitable parameter conditions. Rational lump-type solutions are also constructed, with nonsingularity requiring $\alpha < 0$. The analysis shows that the spatially varying coefficients primarily steer the wave trajectories and modify the interaction geometries, while the exact solutions retain their localized analytical profiles within the admissible parameter regime. These results extend the corresponding constant-coefficient model and enlarge the class of spatially inhomogeneous nonlinear evolution equations exhibiting Painlevé–Hirota coherent-wave structures.

The remainder of the paper is organized as follows. Section 2 presents the Painlevé analysis and derives the Hirota bilinear representation. Section 3 constructs the general N-soliton solution and examines ordinary, resonant, and hybrid nonlinear wave structures. Section 4 derives the rational lump-type solutions, and Section 5 summarizes the principal findings and outlines directions for future research.

2. Painlevé analysis

In this section, we investigate the integrability properties of the proposed nonlinear equation (1.1) by applying the well-known Painlevé analysis. This technique, originally developed by WTC [18], is widely recognized as strong evidence of the Painlevé integrability of the equation. The main objective of the test is to examine whether the solutions of the equation possess only movable pole-type singularities. To carry out the Painlevé analysis, we assume that the solution can be expanded in the form of a Laurent series about the noncharacteristic singularity manifold $\psi(x, y, z, t) = 0$, where $\psi_x \neq 0$ and ψ is analytic. Accordingly, the solution is represented as

$$u = \sum_{j=0}^{\infty} u_j \, \psi^{j+C}, \tag{2.1}$$

where C denotes the leading-order exponent and the coefficients $u_j = u_j(x, y, z, t)$ are analytic functions to be determined recursively. The first step of the WTC procedure is to determine the dominant behavior of the equation. Substituting the above series expansion into the governing equation and balancing the most singular terms yields $C = -2$. This indicates a double-pole leading-order behavior near the movable singularity manifold. Proceeding further, the coefficient corresponding to the leading-order term is obtained as follows:

$$u_0 = 2\psi_x^2. \tag{2.2}$$

The next stage involves calculating the resonance points, which identify the positions where arbitrary functions may enter the series expansion. After substituting the perturbed expansion into the equation and simplifying, the resonance equation becomes

$$\kappa_2(y)\psi_x^4 u_j\,(j-4)\,(j-5)\,(j-6)\,(j+1) = 0. \tag{2.3}$$

Hence, the resonance values are found to be $j = -1,\ 4,\ 5,\ 6$. The resonance $j = -1$ corresponds to the arbitrariness of the singularity manifold $\psi(x, y, z, t)$, while the remaining resonances indicate the locations where arbitrary functions may appear in the Laurent expansion. The recursive computation of the coefficients confirms that the coefficients corresponding to the non-resonant indices are uniquely determined, whereas arbitrary functions emerge at the resonance positions. Setting the coefficients of ψ^{j-6} equal to zero yields u_j, for $j = 1, 2, 3$ as follows:

$$\begin{aligned}
\psi^{-5};\quad u_1 =& 2\psi_{xx},\\
\psi^{-4};\quad u_2 =& -\frac{\kappa_1(y)\psi_t}{6\kappa_2(y)\psi_x} + \frac{3\psi_{xx}^2 - \alpha\psi_t^2 - 4\psi_x\psi_{xxx}}{6\psi_x^2} - \frac{\kappa_3(y)\psi_x + \kappa_4(y)\psi_y + \kappa_5(y)\psi_z}{6\psi_x\kappa_2(y)},\\
\psi^{-3};\quad u_3 =& \frac{(\psi_{xt}\psi_x - \psi_{xx}\psi_t)\,\kappa_1(y)}{6\psi_x^3\kappa_2(y)} + \frac{\alpha\psi_x^2\psi_{tt} - \alpha\psi_t^2\psi_{xx} + \psi_x^2\psi_{xxxx} - 4\psi_x\psi_{xx}\psi_{xxx} + 3\psi_{xx}^3}{6\psi_x^4}\\
&+ \frac{\kappa_4(y)\psi_x\psi_{xy} - \kappa_4(y)\psi_{xx}\psi_y + \kappa_5(y)\psi_{xz}\psi_x - \kappa_5(y)\psi_z\psi_{xx}}{6\psi_x^3\kappa_2(y)},
\end{aligned} \tag{2.4}$$

where $\kappa_2(y) \neq 0$. The recursive computation of the coefficients confirms that the coefficients corresponding to the non-resonant indices are uniquely determined, whereas arbitrary functions emerge at the resonance positions. By setting the coefficients of the corresponding powers of ψ to zero, the remaining compatibility conditions can be examined. In particular, after substituting the expressions for u_1, u_2, and u_3 into the coefficient equation associated with the power ψ^{-2}, the resulting relation is identically satisfied, and the coefficient u_4 remains arbitrary. Similarly, the equations obtained from the coefficients of ψ^{-1} and ψ, which correspond respectively to the resonance levels $j = 5$ and $j = 6$, introduce no additional constraints, and the coefficients u_5 and u_6 also remain arbitrary. Therefore, all resonance conditions are compatible, and no obstruction appears in the Laurent expansion. Consequently, the investigated (3 + 1)-dimensional variable-coefficient extended KdV Eq (1.1) possesses the Painlevé property, providing strong evidence of its integrability and suggesting the existence of rich exact solution structures, including solitons, lump waves, breathers, and other nonlinear wave phenomena. The Painlevé analysis is understood locally on intervals where $\kappa_2(y) \neq 0$. If $\kappa_2(y)$ has isolated zeros, the analysis applies piecewise on the corresponding nondegenerate intervals. The plotted Hirota solutions remain valid wherever their explicit expressions are regular.

Remark 1. *The Painlevé analysis reveals that the integrability of the proposed model is remarkably robust with respect to the choice of the variable coefficients. In particular, the equation successfully* *passes the Painlevé test for arbitrary sufficiently smooth coefficient functions $\kappa_i(y)$, provided that $\kappa_2(y) \neq 0$. The same conclusion is obtained when the coefficients are taken as functions of another spatial variable, i.e., $\kappa_i(z)$, or more generally $\kappa_i(y,z)$. In both cases, the leading-order analysis yields the same dominant behavior with $C = -2$ and $u_0 = 2\psi_x^2$, while the resonance values remain $j = -1, 4, 5, 6$. Although the explicit expressions for the intermediate coefficients u_1, u_2, and u_3 differ from those obtained for the $\kappa_i(y)$ case, the resonance coefficients u_4, u_5, and u_6 remain arbitrary. Hence, all compatibility conditions are satisfied, confirming that the Painlevé property is preserved for coefficient functions depending on z or on the pair of spatial variables (y, z).*

On the other hand, when the coefficients are assumed to depend explicitly on time, i.e., $\kappa_i = \kappa_i(t)$, the leading-order behavior and the resonance values are again found to be identical to those of the main analysis. The recursion relations determine the coefficients u_1, u_2, and u_3, while u_4 and u_5 remain arbitrary. However, unlike the spatially dependent cases, the compatibility condition at the highest resonance is violated, and u_6 is no longer arbitrary unless all coefficient functions reduce to constants. Therefore, the Painlevé property is generally lost for time-dependent coefficients. This indicates that temporal modulation prevents the model from passing the Painlevé test, except in the constant-coefficient limit.

Bilinear representation of the model

We now proceed to derive the Hirota bilinear representation corresponding to Eq (1.1). Since the governing equation has variable coefficients and satisfies the earlier-introduced integrability conditions, it is natural to reformulate it via a dependent-variable transformation suitable for Hirota's direct method. To begin, we introduce the exponential trial function

$$u = e^{\theta}, \qquad \theta = k_i x + p_i(y) + h_i z + w_i t + \xi_i, \tag{2.5}$$

where k_i, h_i, w_i, and ξ_i are arbitrary constants, while $p_i(y)$ remains an unknown function to be determined. Substituting this expression into the linear contribution of Eq (1.1) leads to the following dispersion relation:

$$p_i(y) = \int \left(\frac{-\kappa_2(y)(k_i^4 + \alpha\, w_i^2) - k_i(h_i\kappa_5(y) + k_i\kappa_3(y) + w_i\kappa_1(y))}{k_i\kappa_4(y)} \right) dy, \tag{2.6}$$

where $k_i \neq 0$ and $\kappa_4(y) \neq 0$. Throughout the manuscript, $\int(.)dy$ represents an indefinite integral with respect to y. The associated constants of integration are absorbed into the arbitrary parameters appearing in the phase functions. Next, according to the leading-order term in Painlevé analysis, we employ the logarithmic transformation

$$u = C\,(\ln \mathfrak{g})_{xx}\,, \qquad \mathfrak{g} = 1 + e^{\theta}, \tag{2.7}$$

where $C \neq 0$ is a constant to be fixed later. By inserting this form into Eq (1.1), together with the dispersion relation above, one finds that consistency requires $C = 2$. Consequently, the dependent variable transformation becomes

$$u = 2\,[\ln \mathfrak{g}]_{xx}\,. \tag{2.8}$$

By substituting the dependent variable transformation Eq (2.8) into Eq (1.1), and using $u = \frac{2\mathrm{g}_{xx}}{\mathrm{g}} - \frac{2\mathrm{g}_x^2}{\mathrm{g}^2}$, we express all derivatives of u in terms of derivatives of g. After integrating twice with respect to x, multiplying the resulting equation by g^2, and neglecting the integration constants, we obtain

$$\begin{aligned}&\kappa_1(y)\,(2\mathrm{g}\mathrm{g}_{xt} - 2\mathrm{g}_x\mathrm{g}_t) + \kappa_2(y)\left(2\mathrm{g}_{xxxx}\mathrm{g} - 8\mathrm{g}_{xxx}\mathrm{g}_x + 6\mathrm{g}_{xx}^2\right) + \alpha\,\kappa_2(y)\left(2\mathrm{g}_{tt}\mathrm{g} - 2\mathrm{g}_t^2\right)\\&+ \kappa_3(y)\left(2\mathrm{g}_{xx}\mathrm{g} - 2\mathrm{g}_x^2\right) + \kappa_4(y)\left(2\mathrm{g}\mathrm{g}_{xy} - 2\mathrm{g}_x\mathrm{g}_y\right) + \kappa_5(y)\,(2\mathrm{g}\mathrm{g}_{xz} - 2\mathrm{g}_x\mathrm{g}_z) = 0.\end{aligned} \tag{2.9}$$

To clarify the role of the variable coefficients in this transformation, we note that the functions $\kappa_i(y)$ depend only on the transverse variable y and are independent of x, z, and t. Therefore, when integrating the equation twice with respect to x, these coefficients remain unaffected and no derivatives such as $\kappa_i(y)$ are generated. The variable coefficients simply act as multiplicative factors in the resulting bilinear expression. The resulting expression Eq (2.9) can be recognized as a combination of Hirota bilinear derivatives because each term has the structure generated by D_xD_t, D_x^4, D_t^2, D_x^2, D_xD_y, and D_xD_z, where the Hirota operator is defined through

$$D_x^m D_y^n D_t^p D_z^q(F\cdot G) = (\partial_x - \partial_{x'})^m \left(\partial_y - \partial_{y'}\right)^n (\partial_t - \partial_{t'})^p\, (\partial_z - \partial_{z'})^q\, F(x,y,z,t)G(x',y',z',t')\Big|_{x'=x,\, y'=y,\, z'=z,\, t'=t}. \tag{2.10}$$

Hence, Eq (2.9) can be compactly written as

$$\Big[\kappa_1(y)D_xD_t + \kappa_2(y)D_x^4 + \alpha\,\kappa_2(y)D_t^2 + \kappa_3(y)D_x^2 + \kappa_4(y)D_xD_y + \kappa_5(y)D_xD_z\Big]\mathrm{g}\cdot\mathrm{g} = 0. \tag{2.11}$$

3. Multi-soliton structures

In this section, we restrict attention to $\alpha = 1$ for the construction of the exponential multi-soliton and resonant-wave solutions. The rational lump solutions are treated separately in Section 4, where α is retained explicitly and nonsingularity requires $\alpha < 0$. To derive multi-soliton solutions, we apply Hirota's perturbation expansion. The auxiliary function g is assumed in the form

$$\mathrm{g} = 1 + \epsilon g_1 + \epsilon^2 g_2 + \epsilon^3 g_3 + \cdots + \epsilon^N g_N, \tag{3.1}$$

where ϵ is a bookkeeping parameter and the functions g_j are yet to be determined. Substituting series Eq (3.1) into the bilinear equation (2.11) and collecting coefficients of equal powers of ϵ yields a hierarchy of solvable equations. Following Hirota's standard procedure, the general N-soliton solution can be expressed as

$$u = 2\,[\ln \mathrm{g}]_{xx}\,, \tag{3.2}$$

with

$$\mathrm{g} = \sum_{\mu\in\{0,1\}^N} \exp\left[\sum_{i=1}^{N} \mu_i\theta_i + \sum_{1\le i<j}^{N} \mu_i\mu_j \ln(A_{ij})\right]. \tag{3.3}$$

Here, the summation is taken over all binary vectors

$$\boldsymbol{\mu} = (\mu_1, \mu_2, \ldots, \mu_N), \qquad \mu_i \in 0,1, \quad i = 1,\ldots,N,$$

that is, over all 2^N possible combinations of the binary variables and

$$\theta_i = k_i x + p_i(y) + h_i z + w_i t + \xi_i, \tag{3.4}$$

while the phase functions satisfy

$$p_i(y) = \int \left(\frac{-\kappa_2(y)(k_i^4 + w_i^2) - k_i(h_i\kappa_5(y) + k_i\kappa_3(y) + w_i\kappa_1(y))}{k_i\kappa_4(y)} \right) dy, \tag{3.5}$$

for $k_i \neq 0$ and $\kappa_4(y) \neq 0$. The interaction coefficients are obtained as

$$A_{ij} = \frac{3k_i^2k_j^4 - 6k_i^3k_j^3 + (3k_i^4 - w_i^2)k_j^2 + 2k_ik_jw_iw_j - k_i^2w_j^2}{3k_i^2k_j^4 + 6k_i^3k_j^3 + (3k_i^4 - w_i^2)k_j^2 + 2k_ik_jw_iw_j - k_i^2w_j^2}. \tag{3.6}$$

It can be directly verified that the interaction coefficient satisfies the symmetry property $A_{ij} = A_{ji}$, which is required for the consistency of the Hirota N-soliton solution. Although the expression in Eq (3.6) is written with the indices ordered as (i, j), exchanging i and j leaves the value of the coefficient unchanged.

One-soliton wave

For the simplest case $N = 1$, the auxiliary function reduces to

$$\mathfrak{g} = 1 + e^{\theta_1}, \tag{3.7}$$

where θ_1 is given in Eq (3.4) and the corresponding dispersion relation $p_1(y)$ comes from Eq (3.5). Hence, the one-soliton solution is obtained as

$$u = \frac{k_1^2}{2}\,\mathrm{sech}^2\left(\frac{\theta_1}{2}\right). \tag{3.8}$$

From the one-soliton solution Eq (3.8), it follows that the maximum wave amplitude is attained at $\theta_1 = 0$. Therefore, the peak amplitude is

$$u_{\max} = \frac{k_1^2}{2}, \tag{3.9}$$

showing that the soliton amplitude depends solely on the wave number k_1. In particular, the variable coefficients $\kappa_i(y)$ do not directly affect the amplitude of the solitary wave. The position of the soliton is determined by the condition $\theta_1 = 0$, which yields

$$x = \frac{1}{k_1^2}\left(\int \left[\frac{\left(k_1^4 + w_1^2\right)\kappa_2(y) + h_1k_1\kappa_5(y) + k_1^2\kappa_3(y) + w_1k_1\kappa_1(y)}{\kappa_4(y)} \right] dy - (w_1t + h_1z + \xi_1)k_1 \right), \tag{3.10}$$

where $\kappa_4(y) \neq 0$. This expression demonstrates that the coefficient functions $\kappa_i(y)$ govern the propagation path of the soliton. Consequently, while the amplitude remains unchanged, the trajectory may become curved, oscillatory, or nonuniform depending on the form of the variable coefficients. The above results can be naturally generalized to the multi-soliton solutions. For the two-, three-, and four-soliton cases, each constituent soliton possesses an asymptotic phase function θ_i, and its center is determined by the condition

$$\theta_i = 0, \qquad i = 1, 2, \ldots, N. \tag{3.11}$$

Hence, the individual trajectories of all interacting solitons can be obtained from the corresponding phase functions. Although the interaction coefficients A_{ij} modify the collision dynamics and induce phase shifts during interaction, the asymptotic propagation paths remain governed by the phase relations $\theta_i = 0$. Therefore, the variable coefficients $\kappa_i(y)$ control the trajectories of both single and multiple solitons, whereas the interaction coefficients determine the nature and strength of their mutual interactions.

Figure 1 illustrates the one-soliton solution for several choices of the variable coefficients $\kappa_i(y)$. In all cases, the solution maintains the characteristic bell-shaped localized structure of a solitary wave, demonstrating the robustness of the one-soliton state under both constant and variable coefficient environments. While the amplitude and localized nature of the wave remain essentially unchanged, the propagation path is significantly influenced by the coefficient functions. For the constant-coefficient case shown in Figure 1(a), the corresponding trajectory in Figure 1(d) is given by $x = -2y$, which represents a straight-line propagation with a constant velocity. However, when the coefficients become functions of y, as in Figure 1(b) and (c), the soliton location is no longer described by a linear relation. The trajectories shown in Figure 1(e) and (f) contain trigonometric, exponential, and hyperbolic contributions, resulting in curved propagation paths.

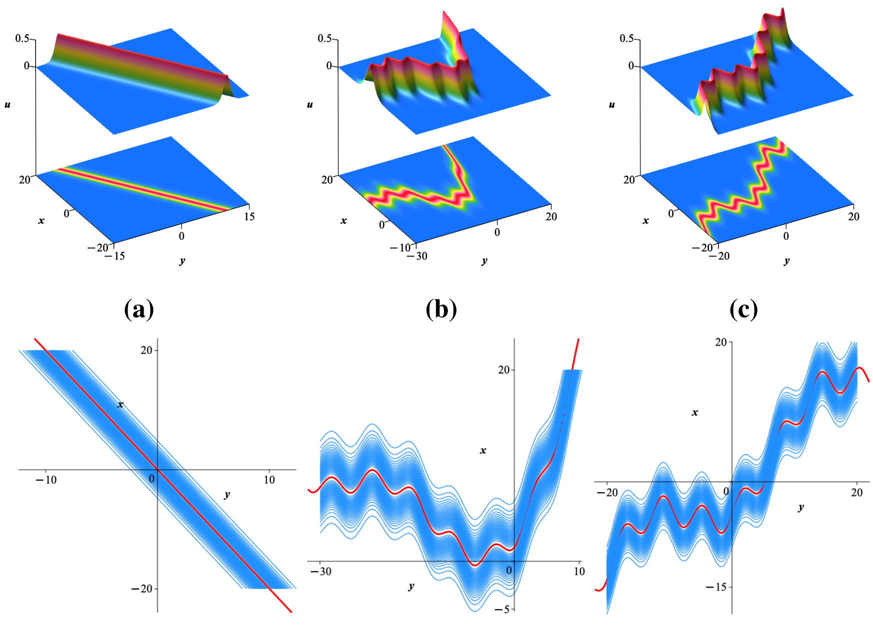

Figure 1. One-soliton solution given by Eq (3.8). (a)–(c) show the localized wave profiles, while (d)–(f) show the corresponding trajectories determined by $\theta_1 = 0$. The common parameters are $h_1 = \frac{2}{3}$, $k_1 = 1$, $\xi_1 = 0$, $w_1 = 1$, and $z = t = 0$. (a), (d): $\kappa_1(y) = -1$, $\kappa_2(y) = -4$, $\kappa_3(y) = 1$, $\kappa_4(y) = 2$, and $\kappa_5(y) = 6$, with $x = -2y$. (b), (e): $\kappa_1(y) = \cos(y/4)$, $\kappa_2(y) = \sin(y)$, $\kappa_3(y) = e^{y/5}$, $\kappa_4(y) = 2$, and $\kappa_5(y) = \tanh(y)$, with $x = 2\sin(y/4) + \frac{5}{2}e^{y/5} - \cos(y) + \frac{1}{3}\ln(\cosh y)$. (c), (f): $\kappa_1(y) = \sin(y/4)$, $\kappa_2(y) = 2\cos(y)$, $\kappa_3(y) = \sin(y/5)$, $\kappa_4(y) = 2$, and $\kappa_5(y) = 2$, with $x = \frac{2y}{3} + 2\sin(y) - 2\cos(y/4) - \frac{5}{2}\cos(y/5)$.

These deviations indicate that the inhomogeneous medium continuously modifies the soliton position during its evolution. An important observation is that the variable coefficients affect only the kinematics of the solitary wave, namely its location and trajectory, while preserving its localized profile. Thus, the one-soliton solution retains its localized profile within the exact solution family as it propagates through the variable medium, while the coefficient functions primarily steer and reshape its propagation path. Figure 2 provides a quantitative characterization of the one-soliton evolution by monitoring the number of wave crests (local maxima) during propagation. In all considered cases, the number of local maxima remains constant throughout the evolution, confirming that the obtained solution preserves its single localized structure despite the presence of spatially varying coefficients. This observation is consistent with the analytical one-soliton solution and demonstrates that the variable coefficients modify only the propagation trajectory without affecting the integrity of the solitary wave.

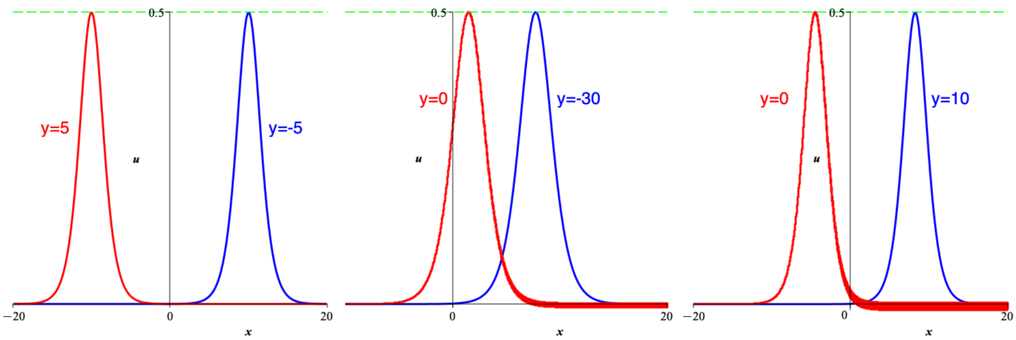

(a) **(b)** **(c)**

Figure 2. One-soliton profiles at selected values of y, showing that the number of wave crests remains unchanged. The parameters in each panel are identical to those used in the corresponding panels of Figure 1.

Two-soliton interaction

For the two-soliton configuration, we consider

$$\mathfrak{g} = 1 + e^{\theta_1} + e^{\theta_2} + A_{12}e^{\theta_1+\theta_2}, \tag{3.12}$$

where θ_i and the interaction parameter A_{12} are given in Eqs (3.4) and (3.6), respectively. Therefore, the resulting two-soliton solution can be written as

$$u = 2\left[\ln\left(1 + e^{\theta_1} + e^{\theta_2} + A_{12}e^{\theta_1+\theta_2}\right)\right]_{xx}. \tag{3.13}$$

Figure 3 illustrates the two-soliton solution Eq (3.13) under different choices of the variable coefficients $\kappa_i(y)$. In all three cases, the solution describes the interaction of two localized solitary waves that preserve their identities after collision, confirming the elastic nature of the interaction. The red and green curves shown in Figure 3(d)–(f) represent the trajectories of the individual solitons obtained from the corresponding phase functions θ_1 and θ_2. For constant coefficients, shown in Figure 3(a), the associated trajectories in Figure 3(d) are straight lines, $x = \frac{106}{75}y + 40$ and $x = -\frac{1727}{1176}y + 20$ indicating uniform propagation of the two solitary waves. In contrast, when the coefficients become variable functions of y, as in Figure 3(b) and (c), the trajectories are no longer linear. The trigonometric and hyperbolic modulations appearing in $\kappa_i(y)$ generate curved propagation paths, as illustrated in Figure 3(e) and (f). These nonlinear trajectories reflect the influence of the inhomogeneous medium on the wave propagation and demonstrate that the variable coefficients continuously modify the soliton position as it evolves.

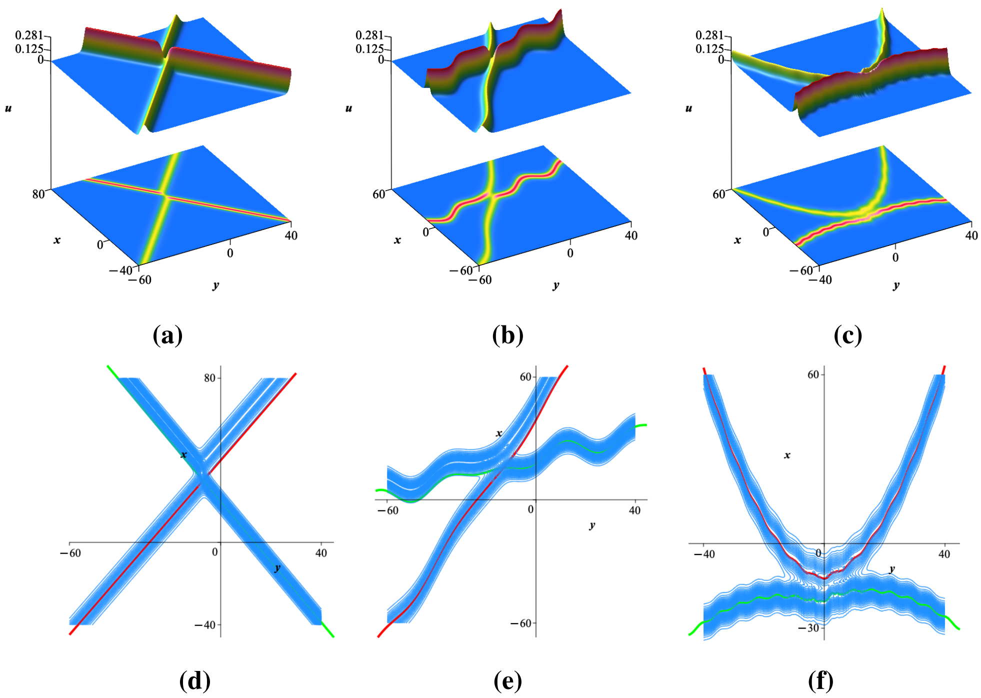

Figure 3. Two-soliton solution given by Eq (3.13). (a)–(c) show the wave profiles, while (d)–(f) show the corresponding trajectories determined by $\theta_1 = 0$ and $\theta_2 = 0$. The common parameters are $h_1 = \frac{2}{3}$, $h_2 = -\frac{1}{3}$, $k_1 = \frac{1}{2}$, $k_2 = \frac{3}{4}$, $\xi_1 = -20$, $\xi_2 = -15$, $w_1 = \frac{1}{5}$, and $w_2 = \frac{4}{7}$. (a), (d) correspond to $(\kappa_1(y), \kappa_2(y), \kappa_3(y), \kappa_4(y), \kappa_5(y)) = (2, -4, 1, 2, 2)$. (b), (e) use $\kappa_1(y) = 2$, $\kappa_2(y) = \sin(y/4)$, $\kappa_3(y) = \cos(y/6)$, $\kappa_4(y) = 2$, and $\kappa_5(y) = 2$. (c), (f) use $\kappa_1(y) = \tanh(y)$, $\kappa_2(y) = 2\sin(y^2/2)$, $\kappa_3(y) = \sin(y)$, $\kappa_4(y) = 2$, and $\kappa_5(y) = \frac{y}{8}$. Red and green curves represent the trajectories associated with $\theta_1 = 0$ and $\theta_2 = 0$, respectively. All plots are evaluated at $z = t = 0$.

An important observation is that the deformation of the trajectories does not alter the fundamental collision mechanism. Although the solitons bend, accelerate, or decelerate along their propagation paths, the interaction remains elastic and the waves recover their localized structures after collision. Therefore, the variable coefficients primarily affect the kinematics of the solitary waves, namely their position and trajectory, while the interaction dynamics continue to be governed by the intrinsic soliton parameters and the interaction coefficient A_{12}. To complement the qualitative visualization of the collision process, Figure 4 presents the evolution of the number of local maxima corresponding to the interactions shown in Figure 3(a). The number of wave crests provides a quantitative measure of the interaction dynamics and enables a direct characterization of the collision process. The obtained results confirm that the interacting solitary waves preserve their identities before and after collision, while the temporary variation in the number of local maxima during the interaction is consistent with the classical geometric description of soliton collisions. Similar quantitative diagnostics based on the evolution of local maxima have recently been employed for nonlinear wave models to characterize overtaking soliton interactions [34]. The present results indicate that the proposed variable-coefficient model exhibits analogous elastic interaction behavior, although the spatially varying coefficients significantly modify the propagation trajectories.

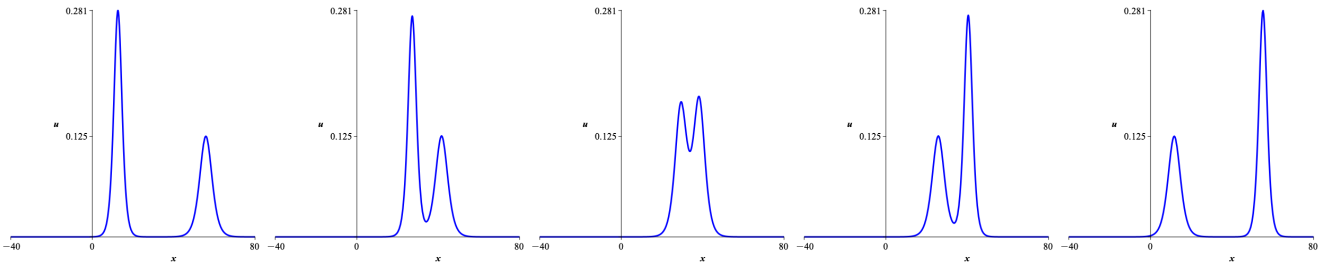

(a) $y = 10$ **(b)** $y = -5$ **(c)** $y = -7.5$ **(d)** $y = -10$ **(e)** $y = -20$

Figure 4. Two-soliton interaction profiles at selected values of y, illustrating the variation in the number of wave crests (local maxima). The parameters are the same as those used in Figure 3(a).

To further understand the role of the interaction coefficient A_{12} appearing in the two-soliton solution Eq (3.13), we present the numerical results shown in Figures 5 and 6. Since A_{12} is determined by the soliton parameters through Eq (3.6), it is not an independent parameter. In the following examples, all parameters are kept fixed except w_1, which is selected so that Eq (3.6) yields the prescribed values $A_{12} = 2$, 10^4, and 10^{10}. The parameter A_{12} multiplies the mixed exponential term $A_{12}e^{\theta_1+\theta_2}$, which represents the nonlinear coupling between the two constituent solitons. Consequently, larger values of the interaction coefficient correspond to stronger nonlinear coupling without affecting the individual dispersion relations of the solitons. In Figure 5, the wave numbers are chosen as $k_1 = -\frac{1}{2}$ and $k_2 = -\frac{2}{3}$, so that both solitons possess the same propagation orientation. As the selected values of w_1 produce progressively larger values of A_{12}, the interaction region becomes increasingly localized and a pronounced central hump emerges. The amplitude of this interaction zone exceeds the amplitudes of the individual solitons, indicating a strong constructive nonlinear superposition. In particular, when the interaction coefficient becomes very large, the mixed interaction term dominates the solution in the overlap region and produces a highly concentrated wave packet. This behavior suggests a temporary concentration of wave amplitude in the interaction region during the collision process.

A markedly different behavior is observed in Figure 6, where $k_1 = -\frac{1}{2}$ and $k_2 = \frac{2}{3}$. In this case, the wave numbers have opposite signs, corresponding to solitons propagating with opposite orientations. Although the selected values of w_1 again produce increasingly larger values of A_{12}, the interaction region remains relatively small and no significant amplification of the wave amplitude occurs. Instead, the collision is characterized mainly by a localized crossing region accompanied by a phase shift. Even for $A_{12} = 10^{10}$, the interaction zone remains much weaker than that observed in Figure 5. The comparison between Figures 5 and 6 reveals that the influence of the interaction coefficient is strongly dependent on the relative propagation directions of the interacting solitons. When the solitons possess wave numbers with the same sign, the nonlinear interaction is cooperative and leads to constructive interference, resulting in a large-amplitude interaction peak. Conversely, when the wave numbers have opposite signs, the interaction is less cooperative, and the energy remains distributed along the individual soliton trajectories rather than being concentrated at the collision center.

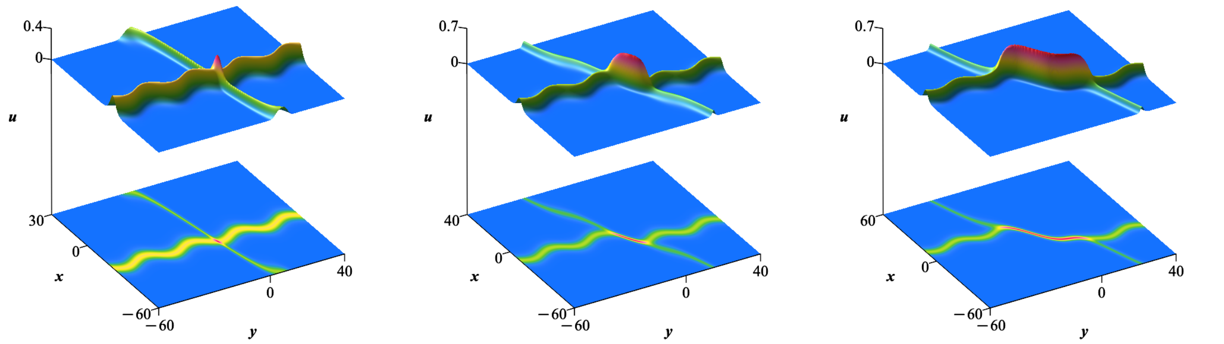

(a) $w_1 = 1.171560176, A_{12} = 2$ **(b)** $w_1 = 0.7604124620, A_{12} = 10^4$ **(c)** $w_1 = 0.7603629710, A_{12} = 10^{10}$

Figure 5. Two-soliton interactions for co-propagating waves ($k_1k_2 > 0$) at increasing values of A_{12}. Larger A_{12} produces a more localized interaction region and a higher central hump. The common parameters are $h_1 = \frac{2}{3}$, $h_2 = \frac{1}{3}$, $k_1 = -\frac{1}{2}$, $k_2 = -\frac{2}{3}$, $\xi_1 = -20$, $\xi_2 = -15$, $w_2 = -\frac{1}{3}$, $\kappa_1(y) = 2$, $\kappa_2(y) = \sin(y/4)$, $\kappa_3(y) = \cos(y/4)$, and $\kappa_4(y) = \kappa_5(y) = 2$, with $z = t = 0$.

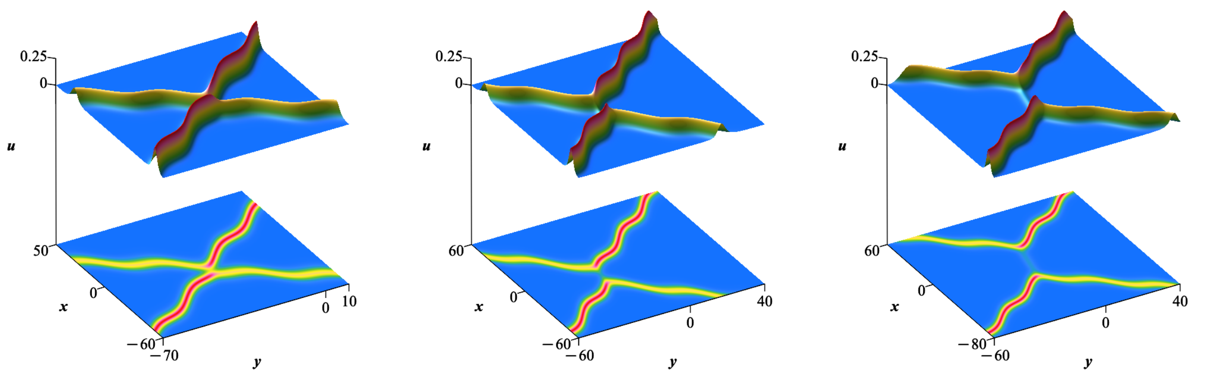

(a) $w_1 = -0.2293803475, A_{12} = 50$ **(b)** $w_1 = -0.1060092943, A_{12} = 10^4$ **(c)** $w_1 = -0.1056624331, A_{12} = 10^{10}$

Figure 6. Effect of the interaction coefficient A_{12} on the collision of oppositely oriented solitons ($k_1k_2 < 0$). In contrast to Figure 5, parameter choices yielding larger values of A_{12} produce a localized crossing region and phase shifts without substantial amplitude amplification. The solitons preserve their localized profiles after interaction, indicating an elastic collision. The common parameters are $h_1 = \frac{2}{3}$, $h_2 = \frac{1}{3}$, $k_1 = -\frac{1}{2}$, $k_2 = \frac{2}{3}$, $\xi_1 = -20$, $\xi_2 = -15$, $w_2 = \frac{1}{3}$, $\kappa_1(y) = 2$, $\kappa_2(y) = \sin(y/4)$, $\kappa_3(y) = \cos(y/4)$, $\kappa_4(y) = 2$, and $\kappa_5(y) = 2$. The plots are obtained at $z = t = 0$.

From a physical point of view, the coefficient A_{12} may be interpreted as a measure of the effective nonlinear coupling strength between two solitary waves. Larger values of A_{12} correspond to stronger interactions and more localized collision regions. However, the resulting wave pattern is not determined by A_{12} alone. The relative signs of the wave numbers play an equally important role. The results of Figure 5 demonstrate that strong nonlinear coupling combined with co-propagating solitons can generate a high-amplitude interaction structure, whereas the results of Figure 6 show that strong coupling between oppositely directed solitons mainly enhances the phase-shift effect without producing substantial amplitude growth.

Therefore, the interaction coefficient A_{12} controls the intensity and localization of the nonlinear interaction, while the wave numbers determine whether the interaction amplitude is concentrated into a large-amplitude collision peak or remains confined to a narrow crossing region. Despite these differences, all collisions remain elastic due to the integrability of the model, and the solitons preserve their identities after interaction.

An important feature of these solutions is that the functions $\kappa_i(y)$ directly influence the nonlinear dispersion relation. Consequently, the resulting wave structures are no longer restricted to the standard straight-line solitons associated with constant-coefficient equations. Depending on the choice of the variable coefficients, the model may exhibit curved trajectories, periodic deformations, or other nontrivial propagation patterns. However, unlike the phase terms, the interaction coefficients A_{ij} are independent of the variable coefficients. This feature can be understood from the Hirota bilinear construction itself. The coefficients A_{ij} arise from the algebraic compatibility conditions obtained when balancing the exponential interaction terms in the bilinear equation. Consequently, they depend only on the intrinsic wave parameters, namely the wave numbers and transverse frequencies, rather than on the temporal modulation functions. More precisely, the quantities A_{ij} determine the interaction mechanism between solitons, including phase shifts and collision properties, whereas the functions $\kappa_i(y)$ govern the evolution of the individual wave phases through the nonlinear dispersion relations. Therefore, the variable coefficients modify the motion and shape of the solitons without changing the fundamental elastic nature of their interactions.

This explains why the collision structure remains elastic even in the presence of variable coefficients. Although the soliton trajectories may bend, stretch, oscillate, or deform due to the influence of $\kappa_i(y)$, the interaction coefficients retain the same mathematical form as in the constant-coefficient case. In other words, the variable coefficients affect the kinematics of the solitons, while the coefficients A_{ij} preserve the intrinsic interaction dynamics inherited from the integrable Hirota framework. These observations demonstrate that the present variable-coefficient model significantly enriches the dynamics of nonlinear wave propagation when compared with its constant-coefficient counterpart. A comparison of Figures 1–6 reveals the influence of increasing the number of interacting solitons on the wave dynamics. Figure 1 illustrates the propagation of a single localized solitary wave, whose trajectory is modified by the variable coefficients while its amplitude and localized profile remain unchanged. In Figure 3, two-soliton interactions exhibit the characteristic elastic collision behavior, where each soliton preserves its identity after interaction with only a phase shift. Figures 5 and 6 demonstrate that the two-soliton interaction pattern depends strongly on the magnitude of the interaction coefficient A_{12} and on the relative signs of the wave numbers. For $k_1k_2 > 0$, increasing A_{12} produces a more localized and pronounced interaction region, whereas for $k_1k_2 < 0$, the collision remains comparatively weak and is characterized mainly by a localized crossing and phase shift. In both cases, the constituent solitons recover their localized profiles after the interaction. These observations indicate that A_{12} controls the intensity and localization of the nonlinear coupling, while the variable coefficients primarily modify the propagation trajectories of the solitary waves.

Three- and four-soliton configuration

Extending the same procedure to $N = 3$ yields the three-soliton expression

$$u = 2\,[\ln \mathfrak{g}]_{xx}\,, \tag{3.14}$$

where

$$\mathfrak{g} = 1 + \mathrm{e}^{\theta_1} + \mathrm{e}^{\theta_2} + \mathrm{e}^{\theta_3} + A_{12}\,\mathrm{e}^{\theta_1+\theta_2} + A_{13}\,\mathrm{e}^{\theta_1+\theta_3} + A_{23}\,\mathrm{e}^{\theta_2+\theta_3} + A_{12}A_{13}A_{23}\,\mathrm{e}^{\theta_1+\theta_2+\theta_3}. \tag{3.15}$$

It is worth emphasizing that the integrability of the present model is further confirmed by the structure of the three-soliton solution. Substituting the perturbation expansion Eq (3.1) into the bilinear equation and collecting terms order by order in ϵ, one finds that the coefficient of the highest-order interaction term $e^{\theta_1+\theta_2+\theta_3}$ is not arbitrary. Instead, consistency of the Hirota expansion requires that this coefficient takes the factorized form $A_{123} = A_{12}A_{13}A_{23}$. This is precisely the three-soliton condition originally established in Hirota's direct method. The absence of any additional constraints among the wave parameters implies that all pairwise interactions are compatible and no higher-order correction terms are required. Consequently, the three-soliton solution is completely determined by the pairwise interaction coefficients. The successful realization of this factorization property demonstrates that the nonlinear interactions satisfy the soliton superposition principle. Therefore, the model possesses the three-soliton property, which is widely recognized as strong additional evidence of integrability. As a result, the construction can be extended recursively to arbitrary N, leading to the general N-soliton solution Eq (3.3). Hence, the presence of Eq (1.1) supports an arbitrary number of interacting solitons and therefore admits the full N-soliton hierarchy.

Extending the same procedure to $N = 4$ yields the four-soliton solution. Owing to its lengthy form, the explicit expression is not presented here and can be obtained directly from the general formula Eq (3.3) by setting $N = 4$. Similar to the three-soliton case, all higher-order interaction terms are completely determined by the pairwise coefficients A_{ij}, and no additional consistency conditions arise. This observation confirms that the Hirota expansion remains valid at higher orders and provides further support for the existence of the general N-soliton solution of the proposed equation. Figures 7 and 8 present the three- and four-soliton solutions, respectively, under different choices of the variable coefficients. In Figure 7, three solitary waves interact within the variable-coefficient medium, producing a complex collision pattern while preserving their individual identities. Although the trajectories are modified by the spatially varying coefficients, the solitons emerge from the interaction without any noticeable change in amplitude or shape, confirming the elastic character of the collision. The variable coefficients mainly influence the propagation paths, leading to bending and deformation of the wave trajectories. Figure 8 further demonstrates the richness of the model through four-soliton interactions. Compared with the three-soliton case, a larger number of interaction regions are formed due to multiple pairwise collisions among the constituent solitons. Despite the increased complexity, the wave structures retain their localized profiles throughout the plotted interactions. The results indicate that the variable-coefficient system preserves the integrable nature of the underlying equation, allowing multiple solitons to interact elastically while exhibiting diverse propagation patterns controlled by the coefficient functions.

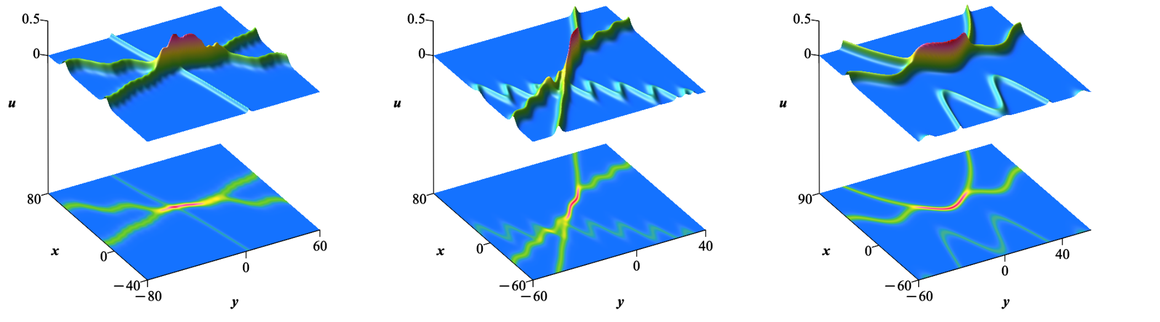

(a) **(b)** **(c)**

Figure 7. Three-soliton solutions for different variable-coefficient settings. The coefficient functions modify the propagation paths and interaction geometry, while the plotted waves retain their localized profiles after successive pairwise interactions. The common parameters are $h_1 = \frac{1}{3}$, $h_2 = \frac{1}{7}$, $h_3 = \frac{1}{5}$, $k_1 = \frac{1}{2}$, $k_2 = -\frac{1}{3}$, $k_3 = -\frac{1}{2}$, $\xi_1 = \xi_2 = -10$, $\xi_3 = 15$, $w_1 = \frac{1}{5}$, $w_2 = 1$, and $w_3 = \frac{2}{3}$. (a) $\kappa_1(y) = \cos(y/5)$, $\kappa_2(y) = -1$, $\kappa_3(y) = 1$, $\kappa_4(y) = 2$, and $\kappa_5(y) = \sin(y)$. (b) $\kappa_1(y) = 2$, $\kappa_2(y) = 2 + \sin(y/2)$, $\kappa_3(y) = 4$, $\kappa_4(y) = 2$, and $\kappa_5(y) = \tanh(y)$. (c) $\kappa_1(y) = \frac{y}{18}$, $\kappa_2(y) = 2 + \sin(y/6)$, $\kappa_3(y) = \frac{y}{10}$, $\kappa_4(y) = 2$, and $\kappa_5(y) = \tanh(y)$. All plots are evaluated at $z = t = 0$.

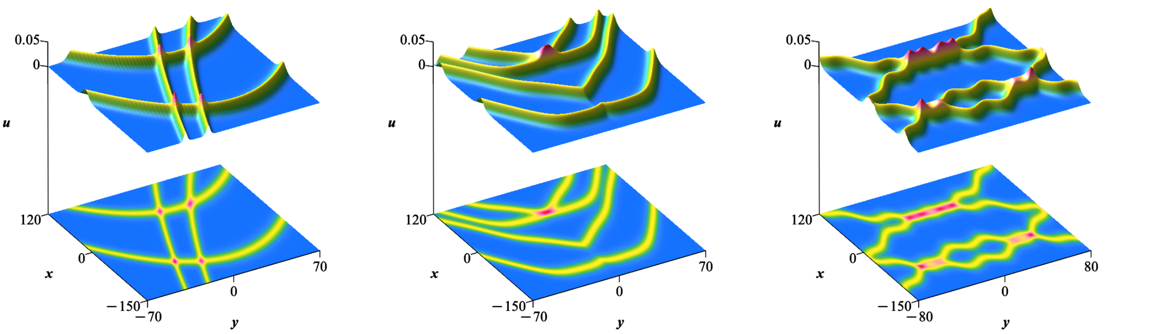

(a) **(b)** **(c)**

Figure 8. Four-soliton interaction patterns for different variable-coefficient environments. The simultaneous interaction of four solitary waves produces multiple collision regions while the constituent waves retain their localized profiles after interaction. The common parameters are $h_1 = \frac{1}{2}$, $h_2 = \frac{3}{4}$, $h_3 = \frac{1}{5}$, $h_4 = \frac{2}{5}$, $k_1 = k_2 = -\frac{1}{5}$, $k_3 = k_4 = \frac{1}{5}$, $\xi_1 = -20$, $\xi_2 = \xi_3 = 10$, $\xi_4 = -10$, $w_1 = -\frac{1}{6}$, $w_2 = 2$, $w_3 = -\frac{1}{3}$, and $w_4 = \frac{2}{5}$. (a) $\kappa_1(y) = \frac{y}{12}$, $\kappa_2(y) = \sin(3y)$, $\kappa_3(y) = 4$, $\kappa_4(y) = 2$, and $\kappa_5(y) = 2$. (b) $\kappa_1(y) = \frac{y}{18}$, $\kappa_2(y) = \sin(y/6)$, $\kappa_3(y) = \frac{y}{10}$, $\kappa_4(y) = 2$, and $\kappa_5(y) = \tanh(y)$. (c) $\kappa_1(y) = \frac{y}{18}$, $\kappa_2(y) = -\frac{y}{16}$, $\kappa_3(y) = \frac{y}{20}$, $\kappa_4(y) = 2$, and $\kappa_5(y) = \sin(y/5)$. All plots are evaluated at $z = t = 0$.

Resonant Y-type, fusion, and fission solitary waves

It is important to note that the multi-soliton solutions obtained through Hirota's bilinear method may generate several resonant interaction patterns under suitable parameter restrictions. In particular, Y-type, fusion, and fission wave structures can be derived from the N-soliton solutions Eq (3.2) when the interaction coefficients satisfy special degeneracy conditions. For the present model, the interaction coefficient is given by

$$A_{ij} = \frac{3k_i^2k_j^4 - 6k_i^3k_j^3 + (3k_i^4 - w_i^2)k_j^2 + 2k_ik_jw_iw_j - k_i^2w_j^2}{3k_i^2k_j^4 + 6k_i^3k_j^3 + (3k_i^4 - w_i^2)k_j^2 + 2k_ik_jw_iw_j - k_i^2w_j^2}. \tag{3.16}$$

Under ordinary parameter selections, one typically has

$$0 < A_{ij} < \infty, \tag{3.17}$$

which corresponds to standard elastic soliton collisions. However, resonant structures arise when the interaction coefficient becomes degenerate. In particular, imposing the condition

$$A_{ij} = 0, \tag{3.18}$$

yields the resonance relation

$$w_j = \frac{k_jw_i}{k_i} \pm \sqrt{3}\, k_j(k_i - k_j). \tag{3.19}$$

Since A_{ij} is a rational function, the resonance condition $A_{ij} = 0$ requires the numerator to vanish while the denominator remains nonzero. Substituting the resulting relation in Eq (3.19) into the denominator shows that it reduces to $12k_i^3k_j^3$, which is nonzero under the standing assumption $k_i \neq 0$ (and hence $k_j \neq 0$ for the interacting solitons). Therefore, no singular cases arise, and Eq (3.19) completely characterizes the resonant condition. Under the constraint in Eq (3.19), the mixed interaction term disappears from the two-soliton expression, and the auxiliary function reduces to

$$\mathfrak{g} = 1 + e^{\theta_1} + e^{\theta_2}. \tag{3.20}$$

As a consequence, the interaction no longer behaves as a conventional elastic collision. Instead, a resonant interaction pattern emerges, producing a Y-shaped wave structure. Physically, this configuration may describe a process in which one incoming soliton splits into two outgoing branches, or conversely, two waves merge into a single localized structure. The same resonance mechanism also gives rise to fusion and fission phenomena. Fusion waves correspond to the process $2 \to 1$, where two solitary waves combine into a single wave after interaction. On the other hand, fission waves correspond to $1 \to 2$, where one localized structure separates into two outgoing waves. Figure 9 shows the reduced two-soliton solution Eq (3.20), which corresponds to a Y-type soliton. As can be seen from the figure, two types of wave interactions are present: fission and fusion solitons. Different values of κ_i are also illustrated in the figure.

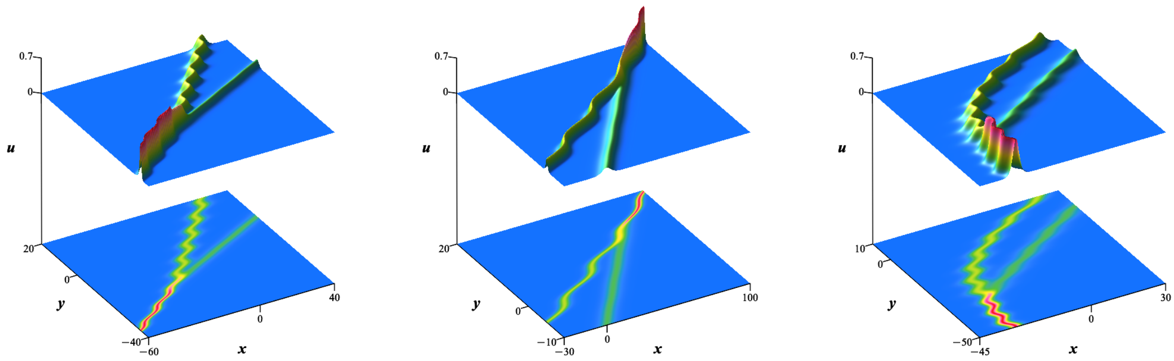

(a) Fission **(b)** Fusion **(c)** Fission

Figure 9. Resonant Y-type solitary-wave solutions obtained under the degeneracy condition $A_{12} = 0$. (a) and (c) show fission processes, in which one incoming wave splits into two outgoing branches, whereas (b) shows a fusion process, in which two incoming waves merge into a single localized wave. The variable coefficients modify the orientation and curvature of the resonant branches while preserving the characteristic Y-shaped structure. The parameters common to all panels are $h_1 = \frac{1}{3}$, $h_2 = -\frac{3}{4}$, $k_1 = \frac{1}{2}$, $k_2 = -\frac{5}{7}$, $\xi_1 = -15$, $\xi_2 = 0$, $w_1 = \frac{1}{5}$, $\kappa_3(y) = 4$, and $\kappa_4(y) = 2$. For (a) and (b), $\kappa_1(y) = 2$, $\kappa_2(y) = \sin(y)$, and $\kappa_5(y) = 2$. For (c), $\kappa_1(y) = \sin(y)$, $\kappa_2(y) = \frac{y}{24}$, and $\kappa_5(y) = 2\cos(y)$. All plots are evaluated at $z = t = 0$.

In general, for the present model Eq (1.1), interactions among several fission and fusion waves can be derived by using the N-soliton solution Eq (3.2), which is summarized as follows:

The nonlinear superposition of M-resonance Y-type solitons and P-resonance Y-type solitons can be obtained from the N-soliton solutions by imposing the parameter conditions

$$A_{ij} = 0, \qquad (1 \le i < j \le M,\ M < i < j \le N,\ N = M + P), \tag{3.21}$$

then

$$w_j = \frac{k_j w_i}{k_i} \pm \sqrt{3}\, k_j (k_i - k_j). \tag{3.22}$$

As an example, when we set $A_{12} = 0$ in the three-soliton solution Eq (3.15), it reduces to the following form:

$$A_{12} = 0, \quad \mathfrak{g} = 1 + \mathrm{e}^{\theta_1} + \mathrm{e}^{\theta_2} + \mathrm{e}^{\theta_3} + A_{13}\, \mathrm{e}^{\theta_1+\theta_3} + A_{23}\, \mathrm{e}^{\theta_2+\theta_3}. \tag{3.23}$$

According to the parameter condition Eq (3.22), two scenarios can be obtained. First, choosing the "−" sign yields a mixed solution consisting of one fission wave and one soliton wave, as shown in Figure 10(a). Second, choosing the "+" sign produces a mixed solution containing one fusion wave and one soliton wave, as shown in Figure 10(b). Similarly, when we set $A_{13} = 0$, we can obtain a mixed solution containing a soliton and fission/fusion waves. For example, for the "+" sign in Eq (3.22), we obtain a hybrid solution consisting of one soliton and one fusion wave, as presented in Figure 10(c).

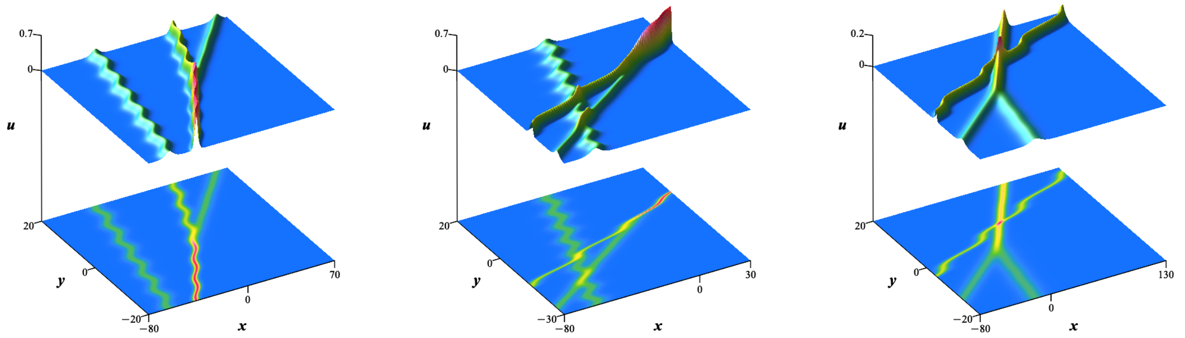

(a) Fission with soliton **(b)** Fusion with soliton **(c)** Fusion with soliton

Figure 10. Hybrid resonant wave structures obtained from the reduced three-soliton solution with one vanishing interaction coefficient. (a) shows the interaction of a fission wave with an ordinary soliton, whereas (b) and (c) show fusion waves coexisting with an ordinary soliton. These configurations demonstrate the coexistence of resonant and non-resonant wave components within the same exact solution. For (a) and (b), the parameters are $h_1 = \frac{1}{3}$, $h_2 = -\frac{3}{4}$, $h_3 = -\frac{1}{3}$, $k_1 = \frac{1}{2}$, $k_2 = -\frac{5}{7}$, $k_3 = -\frac{1}{2}$, $\xi_1 = \xi_2 = 0$, $\xi_3 = -20$, $w_1 = \frac{1}{5}$, $w_3 = 1$, $\kappa_1(y) = 2$, $\kappa_2(y) = \sin(y)$, $\kappa_3(y) = 4$, $\kappa_4(y) = 2$, and $\kappa_5(y) = 2$. For (c), the parameters are $h_1 = \frac{1}{2}$, $h_2 = \frac{7}{4}$, $h_3 = 1$, $k_1 = \frac{1}{2}$, $k_2 = \frac{2}{5}$, $k_3 = \frac{1}{4}$, $\xi_1 = \xi_3 = 0$, $\xi_2 = 20$, $w_1 = \frac{1}{5}$, $w_2 = \frac{3}{2}$, $\kappa_1(y) = 2$, $\kappa_2(y) = \sin(y)$, $\kappa_3(y) = 4$, $\kappa_4(y) = 2$, and $\kappa_5(y) = 2$. All plots are evaluated at $z = t = 0$.

More specifically, when we set $A_{12} = A_{13} = 0$, the three-soliton solution reduces to

$$\mathrm{g} = 1 + \mathrm{e}^{\theta_1} + \mathrm{e}^{\theta_2} + \mathrm{e}^{\theta_3} + A_{23}\,\mathrm{e}^{\theta_2+\theta_3}. \tag{3.24}$$

This reduced form represents a different class of soliton interactions known as X-type solitons. The solution is presented in Figure 11 for different values of κ_i. X-type solitons arise from the oblique interaction of two line solitons, forming a characteristic crossed (X-shaped) wave structure. In this configuration, the interacting solitons retain their identities after collision, exhibiting elastic scattering while undergoing only phase shifts. Physically, such structures are important in nonlinear wave systems because they describe the interaction of coherent wave fronts propagating in different directions, which is commonly observed in fluid dynamics, plasma physics, and optical media [35, 36].

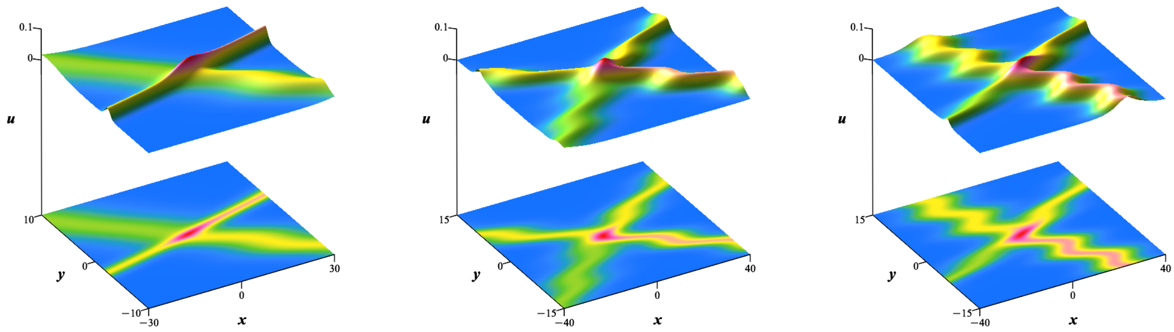

(a) **(b)** **(c)**

Figure 11. X-type soliton solutions derived from the reduced three-soliton configuration with $A_{12} = A_{13} = 0$. The interacting line solitons form characteristic X-shaped patterns and preserve their identities after interaction. The variable coefficients influence the orientation and curvature of the intersecting branches while maintaining the elastic nature of the interaction. The common parameters are $h_1 = \frac{3}{5}$, $h_2 = -\frac{5}{4}$, $h_3 = \frac{5}{2}$, $k_1 = \frac{1}{2}$, $k_2 = \frac{1}{5}$, $k_3 = \frac{1}{4}$, $\xi_1 = \xi_2 = \xi_3 = 0$, and $w_1 = \frac{2}{3}$. In (a), $\kappa_1(y) = 2$, $\kappa_2(y) = \sin(y)$, $\kappa_3(y) = 4$, $\kappa_4(y) = 2$, and $\kappa_5(y) = 2$. In (b), $\kappa_1(y) = \tanh(y/5)$, $\kappa_2(y) = \sin(y)$, $\kappa_3(y) = 5\cos(y)$, $\kappa_4(y) = 2$, and $\kappa_5(y) = -1$. In (c), $\kappa_1(y) = \sin^2(y/5)$, $\kappa_2(y) = 2$, $\kappa_3(y) = 7\cos(y)$, $\kappa_4(y) = 2$, and $\kappa_5(y) = -1$. The plots are shown at $z = t = 0$.

Now we use the four-soliton solution to obtain more complex interaction wave structures. For example, we set some of the phase parameters A_{ij} equal to zero according to the conditions outlined in Eq (3.21). Some representative cases are listed below:

$$
\begin{aligned}
&A_{12} = 0; && \mathfrak{g} = 1 + e^{\theta_1} + e^{\theta_2} + e^{\theta_3} + e^{\theta_4} + A_{13}\, e^{\theta_1+\theta_3} + A_{14}\, e^{\theta_1+\theta_4} + A_{23}\, e^{\theta_2+\theta_3} \\
& && \quad + A_{24}\, e^{\theta_2+\theta_4} + A_{34}\, e^{\theta_3+\theta_4} + A_{13}A_{14}A_{34}\, e^{\theta_1+\theta_3+\theta_4} + A_{23}A_{24}A_{34}\, e^{\theta_2+\theta_3+\theta_4}, \\
&A_{13} = A_{34} = 0; && \mathfrak{g} = 1 + e^{\theta_1} + e^{\theta_2} + e^{\theta_3} + e^{\theta_4} + A_{12}\, e^{\theta_1+\theta_2} + A_{14}\, e^{\theta_1+\theta_4} + A_{23}\, e^{\theta_2+\theta_3} + A_{24}\, e^{\theta_2+\theta_4} \\
& && \quad + A_{12}A_{14}A_{24}\, e^{\theta_1+\theta_2+\theta_4}, \\
&A_{12} = A_{13} = A_{14} = 0; && \mathfrak{g} = 1 + e^{\theta_1} + e^{\theta_2} + e^{\theta_3} + e^{\theta_4} + A_{23}\, e^{\theta_2+\theta_3} + A_{24}\, e^{\theta_2+\theta_4} + A_{34}\, e^{\theta_3+\theta_4} + A_{23}A_{24}A_{34}\, e^{\theta_2+\theta_3+\theta_4}.
\end{aligned}
\tag{3.25}
$$

For the first scenario, we obtain a hybrid solution containing two solitons and one fission/fusion wave. This type of solution is shown in Figure 12 (a). In the second case, the solution forms a mixed structure consisting of one soliton and two Y-type solitons sharing a common branch (a Z-like configuration). This solution is presented in Figure 12 (b). Finally, Figure 12 (c) shows a configuration in which two Y-type solitons interact through their main branches while coexisting with an additional soliton wave, resulting in a more complex mixed-wave structure.

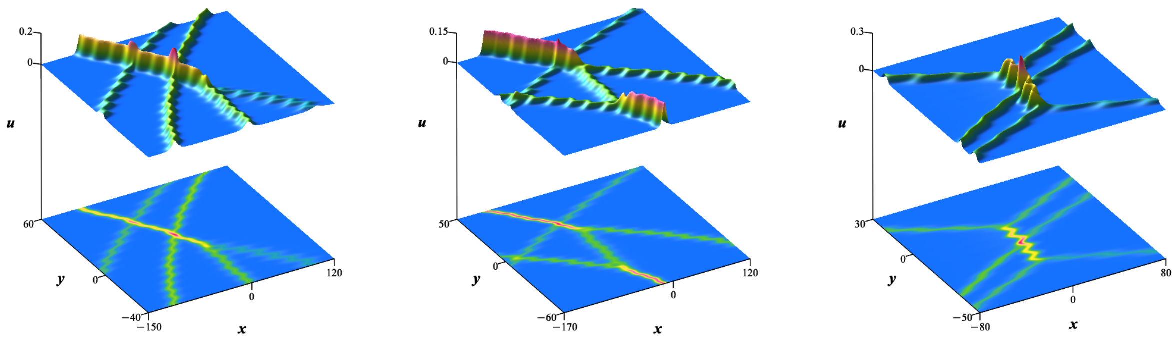

(a) **(b)** **(c)**

Figure 12. Complex hybrid wave structures generated from the four-soliton solution under different resonance constraints. (a) illustrates a Y-type resonant wave interacting with two ordinary solitons. (b) and (c) show configurations consisting of two Y-type resonant structures together with an additional soliton, leading to Z-like shaped and more intricate mixed-wave interaction patterns. The parameter values are as follows. (a): $h_1 = \frac{3}{5}$, $h_2 = \frac{3}{4}$, $h_3 = \frac{5}{2}$, $h_4 = \frac{3}{5}$, $k_1 = -\frac{1}{2}$, $k_2 = -\frac{1}{5}$, $k_3 = \frac{1}{4}$, $k_4 = \frac{1}{3}$, $\xi_1 = \xi_2 = 0$, $\xi_3 = 40$, $\xi_4 = 25$, $w_1 = \frac{2}{3}$, $w_3 = \frac{1}{5}$, $w_4 = \frac{2}{9}$, $\kappa_1(y) = \frac{y}{50}$, $\kappa_2(y) = \sin(y)$, $\kappa_3(y) = \cos(y/3)$, $\kappa_4(y) = 2$, and $\kappa_5(y) = 2$. (b): $h_1 = \frac{7}{8}$, $h_2 = \frac{3}{4}$, $h_3 = \frac{3}{2}$, $h_4 = \frac{3}{8}$, $k_1 = -\frac{1}{2}$, $k_2 = -\frac{1}{4}$, $k_3 = \frac{1}{5}$, $k_4 = \frac{1}{3}$, $\xi_1 = -10$, $\xi_2 = 0$, $\xi_3 = 30$, $\xi_4 = 0$, $w_1 = \frac{2}{3}$, $w_3 = \frac{3}{7}$, $w_4 = \frac{2}{7}$, $\kappa_1(y) = \frac{y}{50}$, $\kappa_2(y) = \sin(y)$, $\kappa_3(y) = \cos(y/3)$, $\kappa_4(y) = 2$, and $\kappa_5(y) = 2$. (c): $h_1 = \frac{5}{8}$, $h_2 = \frac{3}{4}$, $h_3 = \frac{3}{2}$, $h_4 = \frac{3}{7}$, $k_1 = -\frac{1}{3}$, $k_2 = -\frac{1}{4}$, $k_3 = \frac{5}{16}$, $k_4 = \frac{2}{7}$, $\xi_1 = 0$, $\xi_2 = 0$, $\xi_3 = 0$, $\xi_4 = -15$, $w_1 = \frac{2}{3}$, $\kappa_1(y) = 2$, $\kappa_2(y) = \sin(y)$, $\kappa_3(y) = \cos(y/3)$, $\kappa_4(y) = 2$, and $\kappa_5(y) = 2$. The plots are shown at $t = z = 0$.

4. Lump solution structure

In addition to exponential soliton solutions, the variable-coefficient extended KdV Eq (1.1) also admits rationally localized wave structures known as lump waves. Unlike ordinary solitons, which decay exponentially away from their centers, lump solutions exhibit algebraic decay in the (x, y) plane for fixed values of z and t, and therefore represent rationally localized wave structures. Such solutions play an important role in nonlinear wave theory and have been reported in fluid dynamics, plasma physics, nonlinear optics, and other multidimensional physical systems. To derive lump solutions for Eq (1.1), we employ the Hirota bilinear form Eq (2.11) and introduce the quadratic polynomial ansatz

$$\mathfrak{g} = \mathcal{P}_1^2 + \mathcal{P}_2^2 + \delta, \tag{4.1}$$

where δ is a real constant and

$$\mathcal{P}_i = k_i x + \omega_i(y) + h_i z + l_i t + e_i, \quad i = 1, 2.$$

Here, k_i, h_i, l_i, and e_i are arbitrary constants, while $\omega_i(y)$ are functions to be determined. The quadrsuitable for generating lump waves. Substituting expression Eq (4.1) into the bilinear equation (2.11)atic structure of $\mathfrak{g}$ guarantees that the resulting solution is rationally localized and therefore suitable for generating lump waves. Substituting expression Eq (4.1) into the bilinear equation (2.11) and equating coefficients of the independent polynomial terms yields a set of algebraic and differential constraints. After straightforward calculations, the unknown quantities are obtained as

$$\delta = -\frac{3\left(k_1^2 + k_2^2\right)^3}{\alpha\left(l_2 k_1 - k_2 l_1\right)^2}, \tag{4.2}$$

together with

$$\begin{aligned}
\omega_1(y) &= -\int \left(\frac{\alpha\kappa_2(y)\left(k_1\left(l_1^2 - l_2^2\right) + 2k_2 l_1 l_2\right)}{\kappa_4(y)\left(k_1^2 + k_2^2\right)} + \frac{k_1\kappa_3(y) + h_1\kappa_5(y) + l_1\kappa_1(y)}{\kappa_4(y)} \right) dy, \\
\omega_2(y) &= -\int \left(\frac{\alpha\kappa_2(y)\left(k_2(l_2^2 - l_1^2) + 2k_1 l_1 l_2\right)}{\kappa_4(y)\left(k_1^2 + k_2^2\right)} + \frac{k_2\kappa_3(y) + h_2\kappa_5(y) + l_2\kappa_1(y)}{\kappa_4(y)} \right) dy.
\end{aligned} \tag{4.3}$$

The above expressions are valid under the non-degeneracy conditions

$$l_2 k_1 - k_2 l_1 \neq 0, \quad \kappa_4(y) \neq 0. \tag{4.4}$$

The first condition guarantees the existence of a genuinely two-dimensional rational structure, while the second prevents singular behavior in the phase functions $\omega_i(y)$. Consequently, the lump solution of Eq (1.1) can be written as

$$u = 2[\ln(\mathcal{P}_1^2 + \mathcal{P}_2^2 + \delta)]_{xx}. \tag{4.5}$$

To obtain a nonsingular lump solution, the auxiliary function $\mathfrak{g}$ in Eq (4.1) must remain strictly positive. Since $\mathcal{P}_1^2 + \mathcal{P}_2^2 \geq 0$, Eq (4.2) requires $\delta > 0$, which is satisfied if and only if $\alpha < 0$. Therefore, the lump solution Eq (4.5) is nonsingular only for $\alpha < 0$; otherwise, $\mathfrak{g}$ may vanish, leading to singularities in u. The obtained solution represents a localized rational wave whose amplitude decays algebraically away from its center. Unlike line solitons, which extend infinitely along one direction, the lump remains localized in the (x, y) plane for fixed values of z and t, and therefore describes a concentrated wave packet propagating within the inhomogeneous medium. An important feature of solution Eq (4.5) is the role played by the variable coefficients $\kappa_i(y)$. These coefficients enter the solution only through the functions $\omega_1(y)$ and $\omega_2(y)$, which determine the location and trajectory of the lump center. As a result, the variable coefficients do not alter the fundamental rational profile of the lump wave but instead modify its spatial position and propagation path. Depending on the specific forms of $\kappa_i(y)$, the lump may experience bending, displacement, or nonuniform motion while preserving its localized structure. Figure 13 illustrates several lump-wave configurations corresponding to different choices of the coefficient functions. In all cases, the solution exhibits a single localized peak surrounded by algebraically decaying tails. Despite substantial variation in the coefficient functions, the lump retains a qualitatively similar localized profile across the examples shown.

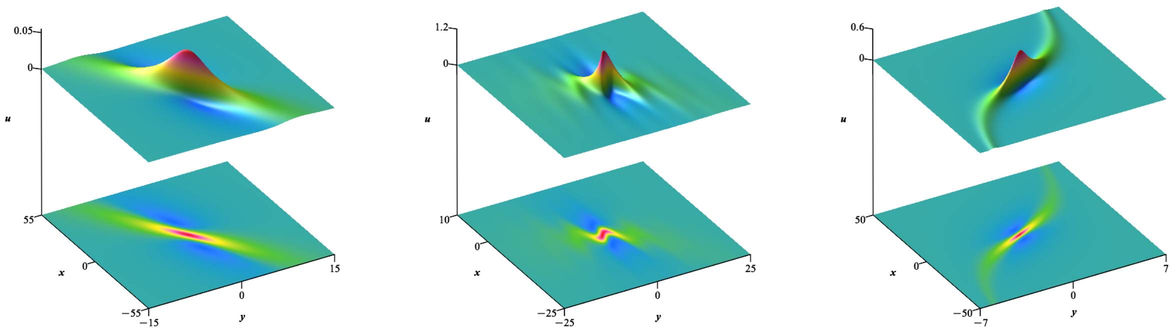

(a) **(b)** **(c)**

Figure 13. Lump solution given by Eq (4.5) for three choices of the variable coefficients $\kappa_i(y)$ at $t = z = 0$. The common parameters are $\alpha = -1$, $k_1 = 1$, $h_1 = 1$, and $e_1 = e_2 = 0$. (a): $k_2 = 2$, $h_2 = 4$, $l_1 = 2$, $l_2 = 3$, $\kappa_1(y) = 2$, $\kappa_2(y) = 5$, $\kappa_3(y) = \cos(y/6)$, $\kappa_4(y) = 1$, and $\kappa_5(y) = 2$. (b): $k_2 = 2$, $h_2 = 1$, $l_1 = -2$, $l_2 = 1/2$, $\kappa_1(y) = 2$, $\kappa_2(y) = -3\cos(y)$, $\kappa_3(y) = e^{y/15}$, $\kappa_4(y) = -2$, and $\kappa_5(y) = \sin(y)$. (c): $k_2 = 3$, $h_2 = 1$, $l_1 = -2$, $l_2 = 1/2$, $\kappa_1(y) = 5/2$, $\kappa_2(y) = \tanh(y/15)$, $\kappa_3(y) = e^{y^2/13}$, $\kappa_4(y) = 1/2$, and $\kappa_5(y) = 2$.

The obtained lump solutions represent rationally localized wave structures propagating through a spatially inhomogeneous medium. The variable coefficients modify the position and trajectory of the lump while its exact profile remains regular under the stated parameter conditions. These solutions complement the exponential soliton and resonant-wave structures obtained earlier and further enrich the exact solution space of the model by demonstrating the coexistence of exponential and rationally localized wave patterns within the same framework.

5. Conclusions

In this work, a variable-coefficient extended KdV equation in (3 + 1)-dimensions was investigated from the perspective of integrability and exact wave structures. By applying the WTC Painlevé analysis, it was shown that the proposed model possesses the Painlevé property and admits the resonance structure required for Painlevé integrability. Based on the leading-order behavior obtained from the singularity analysis, a suitable logarithmic transformation was introduced, which enabled the derivation of the Hirota bilinear representation of the equation. The bilinear formulation was then employed to construct the general N-soliton solution. Explicit one-, two-, three-, and four-soliton solutions were presented and analyzed. The obtained results demonstrate that the variable coefficients mainly influence the propagation paths of the solitary waves, producing curved and nonuniform trajectories, while the localized soliton profiles and elastic collision properties are preserved. Furthermore, the role of the interaction coefficient A_{ij} was examined, showing that it governs the strength and localization of the nonlinear interaction region without altering the integrable nature of the collisions.

Special parameter restrictions were further considered to generate resonant wave structures. Under the degeneracy condition $A_{ij} = 0$, several families of resonant solutions were obtained, including

Y-type solitons, fusion waves, fission waves, X-type solitons, and more complicated hybrid configurations arising from higher-order soliton solutions. These results reveal the rich variety of nonlinear wave interactions supported by the present model. In addition, lump solutions were derived through a quadratic ansatz within the Hirota framework. The resulting rational waves retain localized profiles within the exact solution family, while their positions are affected by the variable coefficients, further enriching the solution space of the equation. Overall, the results indicate that the proposed equation preserves the essential integrable characteristics of the classical KdV-type systems while introducing considerably richer propagation dynamics through spatially varying coefficients. The analytical solutions obtained here may provide useful insight into nonlinear wave phenomena in inhomogeneous media. The variable coefficients were shown to play distinct physical roles in modulating the local propagation speed, the balance between nonlinearity and dispersion, and the transverse coupling of the wave field. The obtained analytical solutions demonstrate that these spatially varying parameters primarily govern the trajectories and interaction geometries of nonlinear waves while preserving their localized character and the integrable nature of the model.

Future investigations may focus on several aspects beyond the scope of the present work. Although the Painlevé property and Hirota bilinear formulation provide strong evidence of integrability, the construction of a Lax pair, Hamiltonian structure, and conservation laws would further establish the integrable nature of the proposed model. The stability and robustness of the exact solutions, particularly the resonant and lump structures, together with the interactions among lump, soliton, breather, and rogue-wave solutions, also deserve further analytical and numerical investigation. Another natural extension is the incorporation of spatial randomness into the variable coefficients to model wave propagation in heterogeneous media. Related studies on nonlinear wave equations with temporal randomness have been reported in [37]. Furthermore, extending the present deterministic multi-soliton framework toward a statistical description of large soliton ensembles within the theory of soliton turbulence, following the pioneering work of Zakharov and the recent review by Didenkulova et al. [38], represents another promising direction for future research.

Author contributions

Majid Madadi: Software, visualization, writing-original draft, methodology, validation, conceptualization; Yakup Yildirim: Software, visualization, writing-original draft, methodology, conceptualization; Udoh Akpan: visualization, writing-original draft, methodology, validation; Lanre Akinyemi: Software, writing-original draft, methodology, validation, conceptualization. All authors have read and approved the final version of the manuscript for publication.

Use of Generative-AI tools declaration

The authors declare they have not used Artificial Intelligence (AI) tools in the creation of this article.

Conflict of interest

The authors declare that they have no conflicts of interest.

References

1. Y. Wang, X. Lü, W. X. Ma, Integrability characteristics and exact solutions of an extended (3 + 1)-dimensional variable-coefficient shallow water wave model, *Nonlinear Dyn.*, **113** (2025), 21725–21741. http://doi.org/10.1007/s11071-025-11268-z
2. X. Y. Gao, Symbolic computation on a (2 + 1)-dimensional generalized nonlinear evolution system in fluid dynamics, plasma physics, nonlinear optics and quantum mechanics, *Qual. Theory Dyn. Syst.*, **23** (2024), 202. http://doi.org/10.1007/s12346-024-01045-5
3. K. K. Ahmed, H. M. Ahmed, T. A. Nofal, T. A. Sulaiman, M. Bayram, Exploration of fractional soliton structures in high-order nonlinear Schrödinger equation in an inhomogeneous optical fiber, *Mod. Phys. Lett. B*, **39** (2025), 2550219. http://doi.org/10.1142/S0217984925502197
4. B. Q. Li, Y. L. Ma, Optical soliton resonances and soliton molecules for the Lakshmanan–Porsezian–Daniel system in nonlinear optics, *Nonlinear Dyn.*, **111** (2023), 6689–6699. http://doi.org/10.1007/s11071-022-08195-8
5. W. X. Ma, Binary Darboux transformation of vector nonlocal reverse-time integrable NLS equations, *Chaos Soliton. Fract.*, **180** (2024), 114539. http://doi.org/10.1016/j.chaos.2024.114539
6. A. Gkogkou, B. Prinari, B. F. Feng, A. D. Trubatch, Inverse scattering transform for the complex coupled short-pulse equation, *Stud. Appl. Math.*, **148** (2022), 918–963. http://doi.org/10.1111/sapm.12463
7. M. Madadi, L. Akinyemi, Localized wave solutions of the second-order Alice–Bob Benjamin–Ono equation via KP-hierarchy reduction, *AIMS Mathematics*, **11** (2026), 10611–10637. http://doi.org/10.3934/math.2026437
8. M. Madadi, M. Inc, M. Bayram, Nonlinear wave behaviors for a combined Kadomtsev–Petviashvili–Boiti–Leon–Manna–Pempinelli equation in fluid dynamics, plasma physics and nonlinear optics, *Wave Motion*, **139** (2025), 103584. http://doi.org/10.1016/j.wavemoti.2025.103584
9. J. Sabiú, S. Sirisubtawee, M. Inc, S. Rezapour, New solitary wave solutions for two (3 + 1)-dimensional extended Kairat-type equations via the generalized Riccati equation method, *Mod. Phys. Lett. A*, **40** (2025), 2550079. http://doi.org/10.1142/S0217732325500798
10. L. Akinyemi, I. Ainomugisha, Stability and solitary wave dynamics of higher-dimensional nonlinear Schrödinger equation with time-dependent potential, *Nonlinear Dyn.*, **113** (2025), 23439–23456. http://doi.org/10.1007/s11071-025-11325-7
11. F. N. K. Sağlam, B. Kopçasız, L. Akinyemi, Analytical approaches to the Kaup–Newell model in mathematical physics, *Mod. Phys. Lett. B*, **40** (2026), 2550271. http://doi.org/10.1142/S0217984925502719
12. J. Ahmad, S. Akram, K. Noor, M. Nadeem, A. Bucur, Y. Alsayaad, Soliton solutions of fractional extended nonlinear Schrödinger equation arising in plasma physics and nonlinear optical fiber, *Sci. Rep.*, **13** (2023), 10877. http://doi.org/10.1038/s41598-023-37757-y
13. A. Ozkan, On the soliton solutions of some time conformable equations in fluid dynamics, *Int. J. Mod. Phys. B*, **38** (2024), 2450027. http://doi.org/10.1142/S0217979224500279

14. S. Kumar, B. Mohan, R. Kumar, Lump, soliton, and interaction solutions to a generalized two-mode higher-order nonlinear evolution equation in plasma physics, *Nonlinear Dyn.*, **110** (2022), 693–704. http://doi.org/10.1007/s11071-022-07647-5

15. Q. Zhou, Z. Huang, Y. Sun, H. Triki, W. Liu, A. Biswas, Collision dynamics of three-solitons in an optical communication system with third-order dispersion and nonlinearity, *Nonlinear Dyn.*, **111** (2023), 5757–5765. http://doi.org/10.1007/s11071-022-08138-3

16. C. H. Feng, B. Tian, X. T. Gao, Bilinear Bäcklund transformations, as well as N-soliton, breather, fission/fusion and hybrid solutions for a (3 + 1)-dimensional integrable wave equation in a fluid, *Qual. Theory Dyn. Syst.*, **24** (2025), 100. http://doi.org/10.1007/s12346-025-01241-x

17. W. X. Ma, Y. Zhou, Lump solutions to nonlinear partial differential equations via Hirota bilinear forms, *J. Differ. Equ.*, **264** (2018), 2633–2659. http://doi.org/10.1016/j.jde.2017.10.033

18. J. Weiss, M. Tabor, G. Carnevale, The Painlevé property for partial differential equations, *J. Math. Phys.*, **24** (1983), 522–526. http://doi.org/10.1063/1.525721

19. R. Grimshaw, *Internal solitary waves*, In: *Environmental stratified flows*, Boston: Springer, 2003, 1–27. http://doi.org/10.1007/0-306-48024-7_1

20. V. N. Serkin, A. Hasegawa, Novel soliton solutions of the nonlinear Schrödinger equation model, *Phys. Rev. Lett.*, **85** (2000), 4502–4505. http://doi.org/10.1103/PhysRevLett.85.4502

21. R. Grimshaw, E. Pelinovsky, O. Poloukhina, Higher-order Korteweg–de Vries models for internal solitary waves in a stratified shear flow with a free surface, *Nonlinear Proc. Geoph.*, **9** (2002), 221–235. http://doi.org/10.5194/npg-9-221-2002

22. Y. S. Kivshar, G. P. Agrawal, *Optical solitons: From fibers to photonic crystals*, San Diego: Academic Press, 2003. http://doi.org/10.1016/B978-0-12-410590-4.X5000-1

23. L. A. Ostrovsky, A. I. Potapov, *Modulated waves: Theory and applications*, Baltimore: Johns Hopkins University Press, 2003.

24. H. F. Ismael, T. A. Sulaiman, H. R. Nabi, S. F. Ahmed, Novel nonlinear dynamical solutions to the (2 + 1)-dimensional variable-coefficients equation arising in oceanography, *Eng. Rep.*, **7** (2025), e70240. http://doi.org/10.1002/eng2.70240

25. X. Y. Gao, In plasma physics and fluid dynamics: Symbolic computation on a (2 + 1)-dimensional variable-coefficient Sawada–Kotera system, *Appl. Math. Lett.*, **159** (2025), 109262. http://doi.org/10.1016/j.aml.2024.109262

26. X. Y. Xie, G. Q. Meng, Dark solitons for a variable-coefficient AB system in the geophysical fluids or nonlinear optics, *Eur. Phys. J. Plus*, **134** (2019), 359. http://doi.org/10.1140/epjp/i2019-12726-7

27. A. M. Wazwaz, W. Alhejaili, R. T. Matoog, S. A. El-Tantawy, Painlevé integrability and multiple soliton solutions for the extensions of the (modified) Korteweg–de Vries-type equations with second-order time derivative, *Alex. Eng. J.*, **103** (2024), 393–401. http://doi.org/10.1016/j.aej.2024.08.052

28. K. J. Wang, B. R. Zou, H. W. Zhu, S. Li, G. Li, Phase portrait, bifurcation and chaotic analysis, variational principle, Hamiltonian, novel solitary, and periodic wave solutions of the new extended Korteweg–de Vries-type equation, *Math. Methods Appl. Sci.*, **48** (2025), 9901–9909. http://doi.org/10.1002/mma.10852

29. T. Anwar, C. Xu, M. A. Khan, Dynamical analysis, synchronization of chaos, and soliton solutions of a nonlinear (3 + 1)-dimensional extension of KdV equation with second-order time derivative, *Chaos Soliton. Fract.*, **207** (2026), 117992. http://doi.org/10.1016/j.chaos.2026.117992

30. M. Madadi, M. Inc, S. Gulsen, H. Bicer, L. Akinyemi, Determinant solitons and rational lump waves in a (3 + 1)-dimensional extended Korteweg–de Vries equation, *Wave Motion*, **147** (2026), 103782. http://doi.org/10.1016/j.wavemoti.2026.103782

31. J. Chu, X. Chen, Y. Liu, Integrability, lump solutions, breather solutions and hybrid solutions for the (2 + 1)-dimensional variable-coefficient Korteweg–de Vries equation, *Nonlinear Dyn.*, **112** (2024), 619–634. http://doi.org/10.1007/s11071-023-09062-w

32. E. Yomba, Construction of new soliton-like solutions for the (2 + 1)-dimensional KdV equation with variable coefficients, *Chaos Soliton. Fract.*, **21** (2004), 75–79. http://doi.org/10.1016/j.chaos.2003.09.028

33. M. Wang, J. Zhang, Z. Liu, E. Li, Soliton-like solutions of general variable-coefficient (2 + 1)-dimensional KdV equation with linear damping term, *Appl. Math. Lett.*, **129** (2022), 107929. http://doi.org/10.1016/j.aml.2022.107929

34. M. V. Flamarion, Solitary wave collisions for the Whitham equation, *Comput. Appl. Math.*, **41** (2022), 356. http://doi.org/10.1007/s40314-022-02076-x

35. N. N. Akhmediev, A. Ankiewicz, *Solitons: Non-linear pulses and beams*, New York: Springer, 1997.

36. D. V. Skryabin, A. V. Gorbach, Colloquium: Looking at a soliton through the prism of optical supercontinuum, *Rev. Mod. Phys.*, **82** (2010), 1287–1299. http://doi.org/10.1103/RevModPhys.82.1287

37. M. V. Flamarion, E. Pelinovsky, E. Didenkulova, Soliton dynamics in random fields: The Benjamin–Ono equation framework, *Appl. Math. Model.*, **144** (2025), 116092. http://doi.org/10.1016/j.apm.2025.116092

38. E. Didenkulova, M. V. Flamarion, E. Pelinovsky, KdV-like soliton gas: Similarity and difference in integrable and non-integrable models, *Physica D*, **481** (2025), 134815. http://doi.org/10.1016/j.physd.2025.134815